CHAPTER 4

RESULTS AND DISCUSSIONS

4.1 Physical Appearances

Figure 4.1 to Figure 4.6 show free standing 3D printed PUA gel polymer electrolytes with different $LiClO_4$ concentration (wt.%). The electrolytes were successfully printed using stereolithography technique into thin film polymer electrolytes with consistent dimensions of 1.89 cm diameter and 0.05 cm thickness. The 3D printed PUA GPEs were flexible, and the transparency of the polymer electrolytes changed in each salt concentration. The incorporation of $LiClO_4$ and DMF into PUA polymer initially turned the GPEs cloudy. However, further addition of 15, 20, and 25 wt.% $LiClO_4$ results in a counterintuitive trend, as the samples progressively became more transparent accordingly.

Figure 4.1: 0 wt.% $LiClO_4$ 3D Printed GPEs

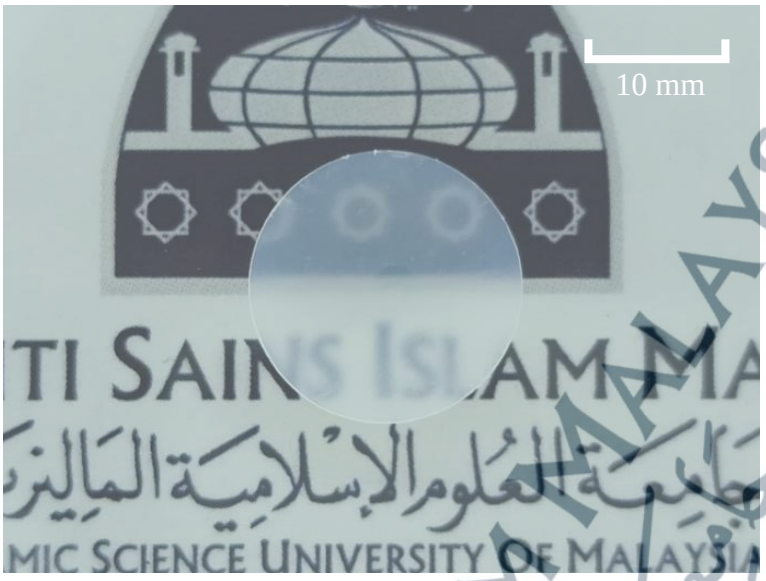

Figure 4.2: 5 wt.% $LiClO_4$ 3D Printed GPEs

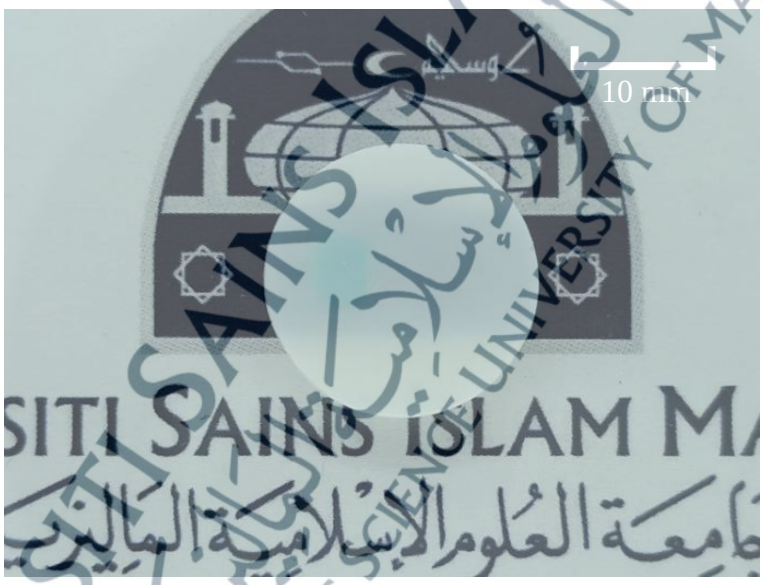

Figure 4.3: 10 wt.% $LiClO_4$ 3D Printed GPEs

Figure 4.4: 15 wt.% $LiClO_4$ 3D Printed GPEs

Figure 4.5: 20 wt.% $LiClO_4$ 3D Printed GPEs

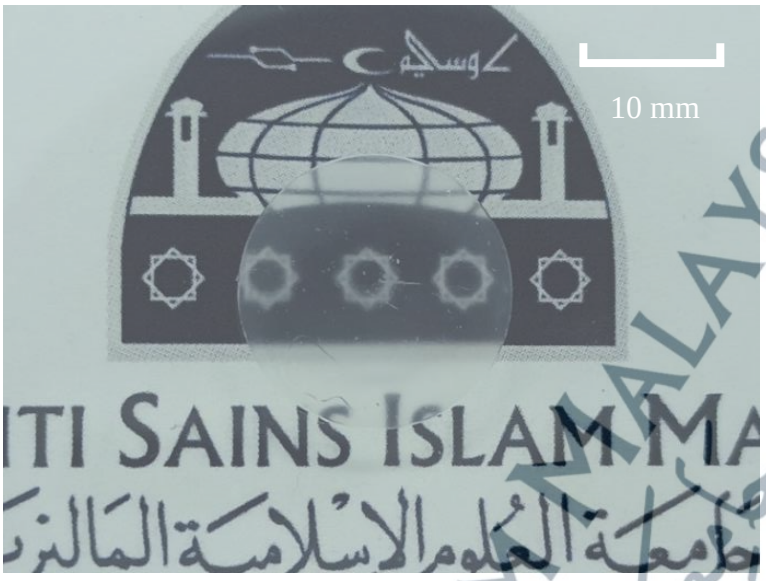

Figure 4.6: 25 wt.% $LiClO_4$ 3D Printed GPEs

Figure 4.7: Flexibility of The 3D Printed GPEs

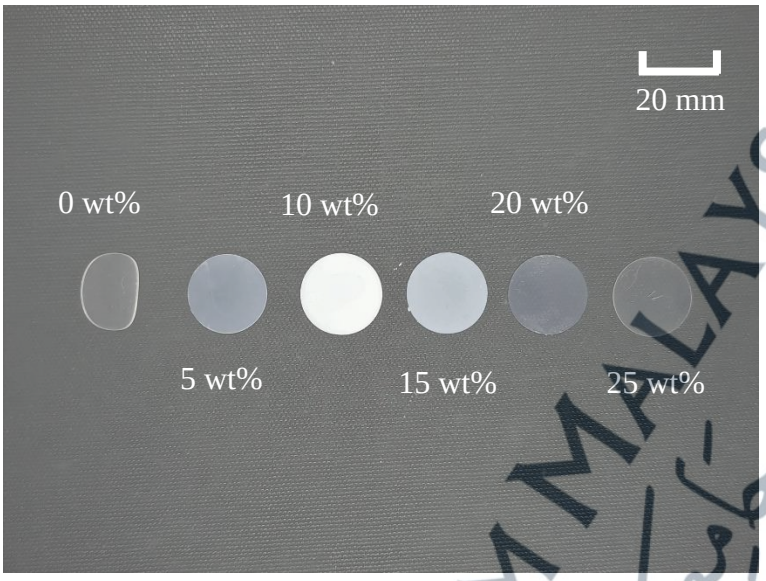

Figure 4.8 : Side by Side Comparison of All GPEs Samples

The differences in transparency of the 3D printed GPEs samples are shown in Figure 4.8 and can be ranked from the cloudiest as follows: 10 wt.% >15 wt.% > 5 wt.% > 20 wt.% > 25 wt.% > 0 wt.%. This trend suggests that the presence of more gel polymer electrolyte material leads to increased cloudiness. This observation can be attributed to the formation of micropores within the material. Micropores are small holes or pores within the gel polymer electrolyte that can scatter or absorb light. When a higher number of micropores are present, they can scatter light to a greater extent, resulting in reduced overall transparency. This finding is consistent with previous research by Tang et al. (2020) who demonstrated that the presence of dispersed pores within a polymer can have a light-scattering effect and reduce transparency. Besides, Harshlata et al. (2021) stated that the white color ionic liquid based nanocomposite GPE in their study was because of the porous nature of the membranes.

The porosity or pores within GPEs facilitates the transport of ions between the electrodes, which is crucial for the proper functioning of the battery. These interconnected

pores act as pathways for the movement of ions which allow them to flow freely from one electrode to the other during the charge and discharge cycles. The present of the pores within the GPEs can be seen through the scanning electron microscope.

4.2 Scanning Electron Microscope (SEM)

Figure 4.9 illustrates the microstructure of 3D printed PUA GPEs with different concentration of $LiClO_4$ from the SEM. The 3D printed 0 wt.% GPEs was observed to have a very smooth surface as shown in Figure 4.9 (a). However, the addition of $LiClO_4$ into the system changed the morphological structure as seen in Figure 4.9 (b)-(f) and the changes are seen to be different according to the amount of $LiClO_4$. The GPEs surface became coarse after the addition of 5 wt.% and coarser after 10 wt.% $LiClO_4$ added. However, the coarse surface was reduced to 15 wt.% and the becoming smoother at 20 wt.% and 25 wt.%. These changes indicated there were structural rearrangements that might occurred within the polymer chain which could affect the Li^+ ions transport within the polymer matrix (Ramesh et al., 2010).

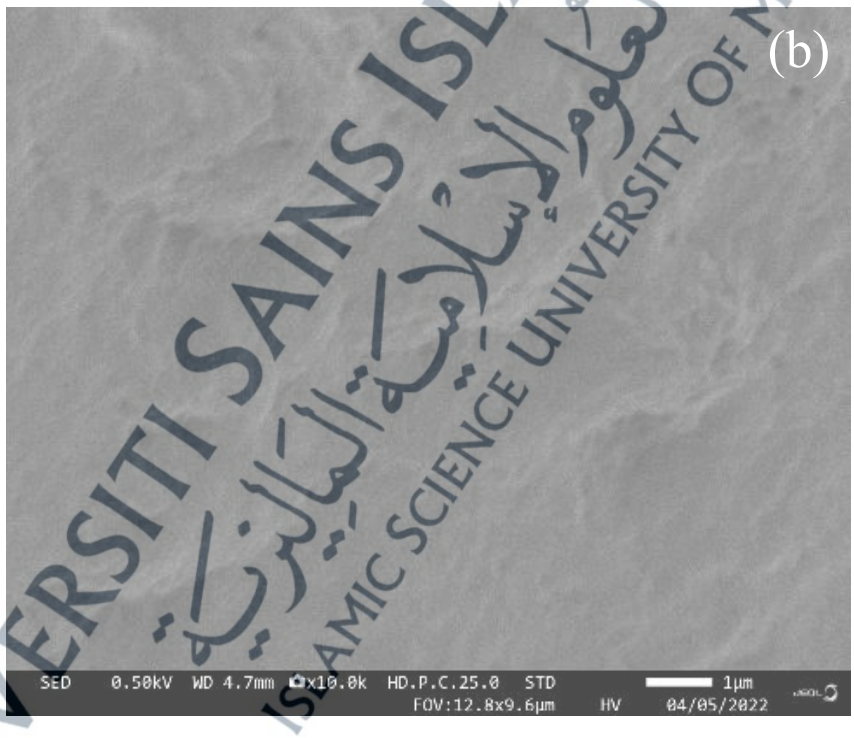

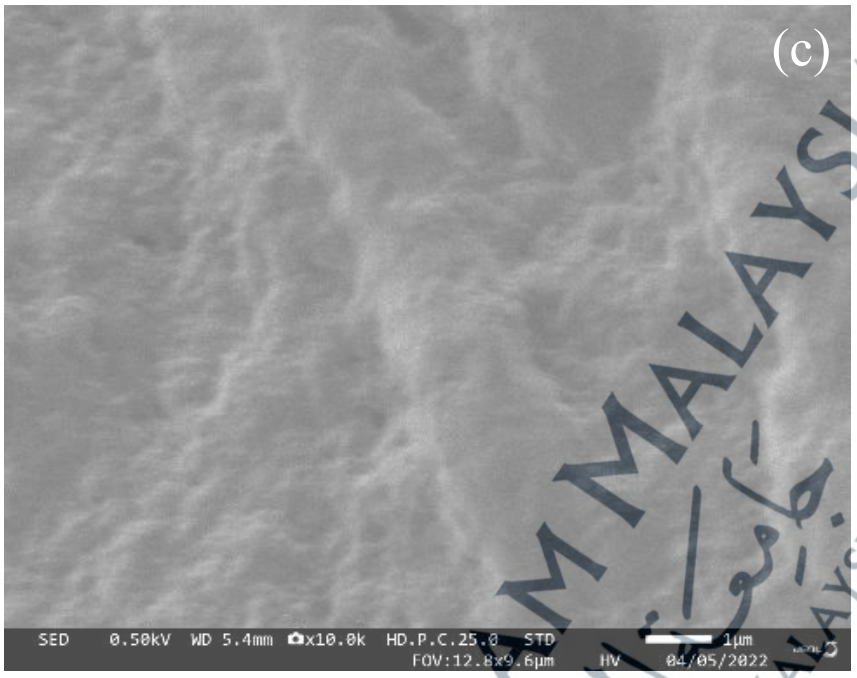

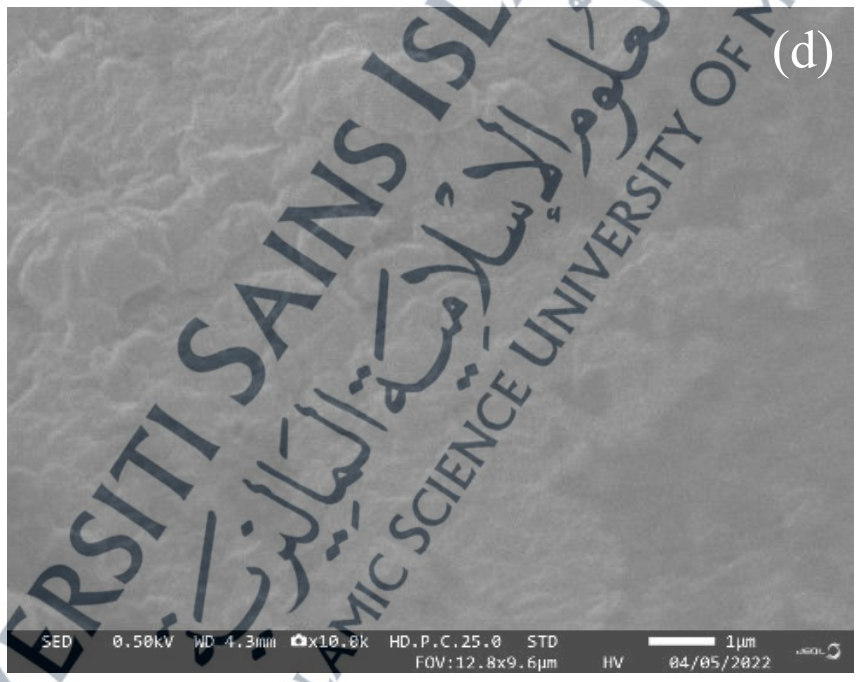

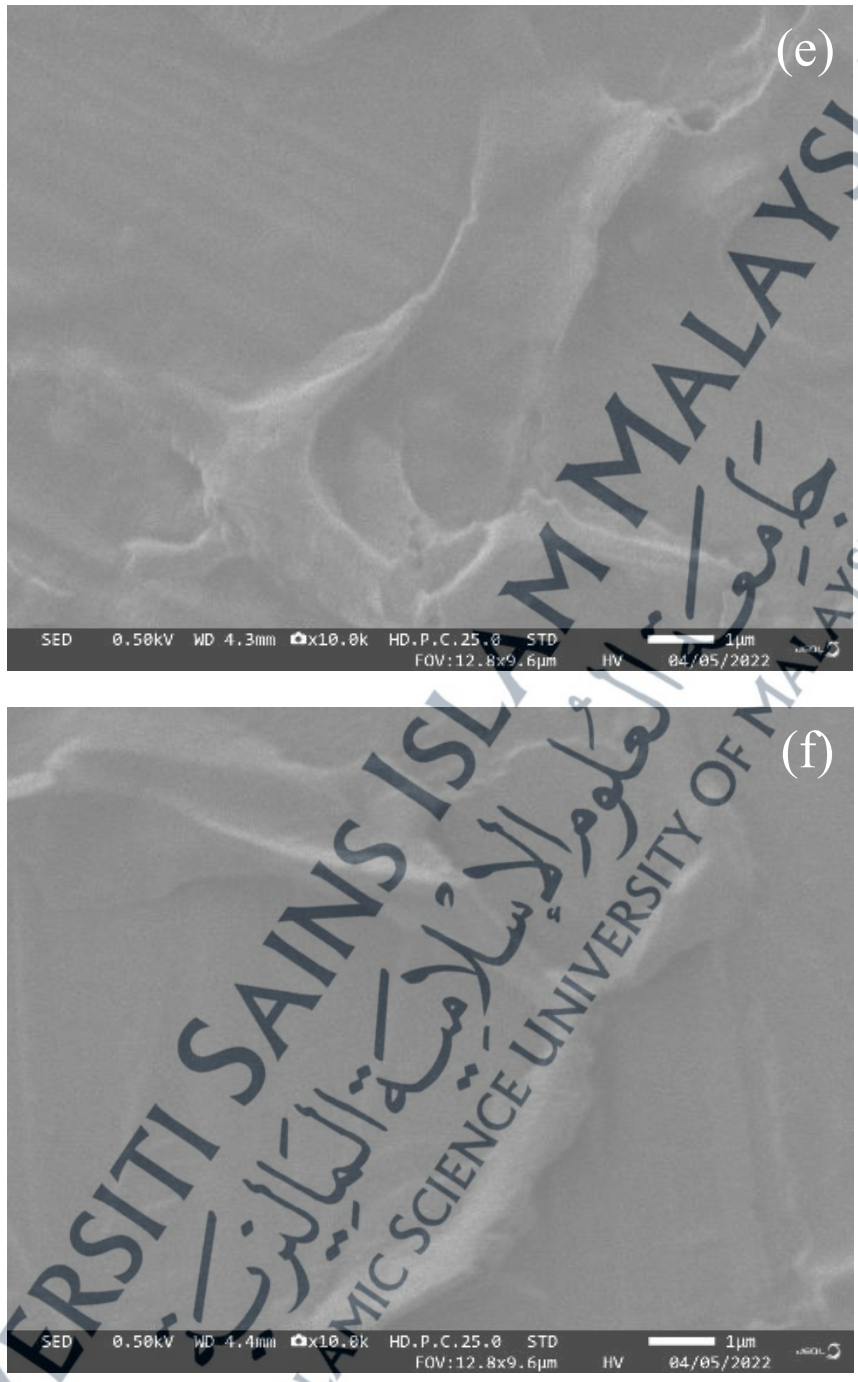

Figure 4.9: The Morphology of Different $LiClO_4$ Concentration PUA GPEs Produced Through SLA Printing. FTIR Deconvolution of $LiClO_4$ Peak (650 - 600 cm-1); (a) 0 wt.%, (b) 5 wt.%, (c) 10 wt.%, (d) 15 wt.%, (e) 20 wt.% and (f) 25 wt.%

4.3 X-ray Diffraction Analysis (XRD)

X-ray diffraction (XRD) analysis was utilized to explore the crystalline characteristics of the polymer material. Figure 4.10 presents the XRD patterns of the PUA GPEs generated via 3D printing, encompassing $LiClO_4$ concentrations ranging from 0 wt.% to 25 wt.%. The XRD patterns offer valuable insights into the structural arrangement and crystallinity of the polymer material, providing information on how the incorporation of $LiClO_4$ at various concentrations influences the crystalline properties of the GPEs.

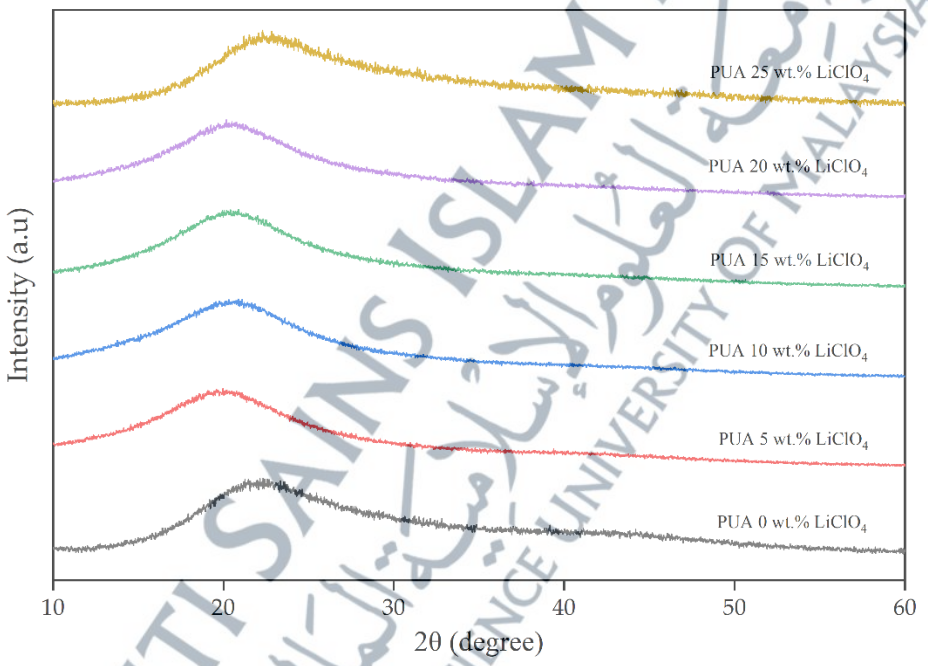

Figure 4.10: XRD Pattern of 3D Printed PUA GPEs Samples From 0 wt.% To 25 wt.% $LiClO_4$ Concentration

According to Figure 4.10,

Broad humps were observed at 15° to 30° for all GPE samples, indicating their amorphous nature without any crystalline peaks. When 5 wt.% $LiClO_4$ was added to the PUA sample, a shift to lower angles (leftward) was observed at a 2θ angle of 22°. As the amount of $LiClO_4$ increased, the peak shifted progressively to higher angles (rightward),

peaking at 25 wt.% $LiClO_4$. This significant shift at 25 wt.% $LiClO_4$ is attributed to the higher salt concentration. The peak corresponding to $LiClO_4$ was not visible, indicating its complete dissolution in the PUA electrolyte (Imperiyka et al., 2014).

The interaction between the lithium salt and the polymer matrix can also impact the electrolyte's conductivity. This interaction GPEs is primarily through ion-dipole interactions and coordination complexes. When lithium salt is added to the polymer matrix, the lithium ions interact with the polar groups such as oxygen atoms present in the polymer chains. This interaction leads to the formation of coordination complexes, where the lithium ions are surrounded by polymer chains.

This interaction can alter the quantity of free space within the polymer, thereby increasing the amorphous phase of the GPEs. The amorphous phase is important because it has a higher ionic conductivity than the crystalline phase. This is because the polymer chains in the amorphous phase have a greater degree of motion and bond rotation, which allows ions to move more freely and improve conductivity. An augmentation in the amorphous phase reduces the energy barrier for segmental motion in the GPE, which facilitates the movement of ions and leads to an additional improvement in conductivity (Johan et al., 2011).

Table 4.1: FWHM of 3D Printed PUA GPEs with vary $LiClO_4$ Concentration

Compositions	Centre 2θ	Area	Full width at half maximum (FWHM)
0 wt.% $LiClO_4$	22.92	6889.50	9.79
5 wt.% $LiClO_4$	19.79	22101.93	12.49
10 wt.% $LiClO_4$	20.36	24151.16	13.72
15 wt.% $LiClO_4$	20.13	13145.70	9.48
20 wt.% $LiClO_4$	20.95	11006.64	9.25
25 wt.% $LiClO_4$	22.96	3060.93	7.36

The correlation between the concentration of $LiClO_4$ in the polymer electrolyte and the full width at half maximum (FWHM) of the XRD hump is presented in Table 4.1 and Figure 4.11. A high FWHM value implies a significant proportion of amorphous polymer in the GPEs. According to the FWHM analysis, the FWHM value of the XRD hump increased until the $LiClO_4$ concentration reached 10wt.%, after which it started to decline at higher concentrations. This implies that the maximum quantity of amorphous material is present in the GPE at a $LiClO_4$ concentration of 10 wt.%, and it decreases at concentrations beyond that point.

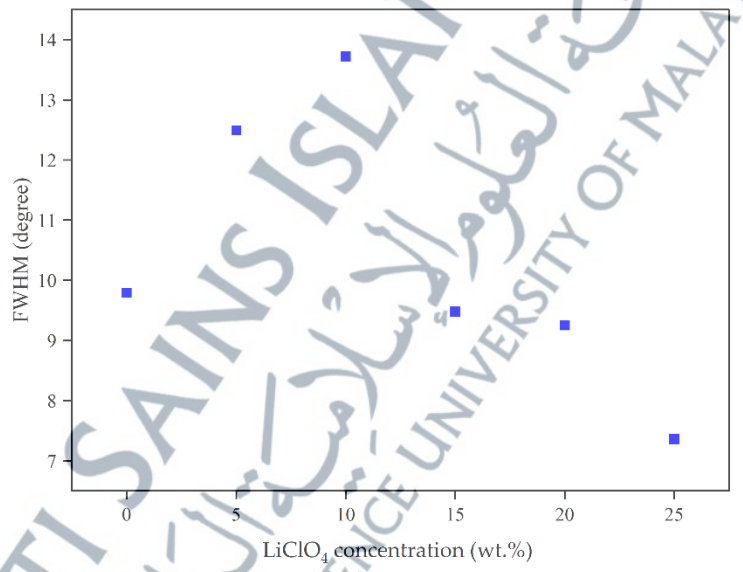

Figure 4.11: FWHM of PUA GPEs Samples with The $LiClO_4$ Concentration

The FWHM value, which indicates the quantity of amorphous material in the polymer electrolyte, corresponds to the pattern of ionic conductivity measured by EIS. The ionic conductivity of the electrolyte increases only until a $LiClO_4$ concentration of 10wt.%, after which it starts to decline at higher concentrations. This indicates that the presence of a certain amount of amorphous phase is advantageous for the electrolyte's conductivity.

4.4 Fourier Transform Infrared Spectroscopy (FTIR)

Figure 4.12 depicted the FTIR spectrum for samples of 0 wt.%, 5 wt.%, 10 wt.%, 15 wt.%, 20 wt.% and 25 wt.%. The changes of peak intensity and band shift in the functional of the carbonyl group (C=O) at 1725-1650 cm^{-1}, -NH stretching mode at 3800–3100 cm^{-1}, and ester group (C-O-C) at 1300-1000 cm^{-1} are observed. These functional groups are chosen because they are expected to be sensitive indicators of the interactions between Li^+ ions and the functional groups in the GPEs. The lithium ion could have interaction with nitrogen and oxygen atoms (Chai et al., 2020).

The changes in the peak spectrum of these functional groups with the addition of lithium salt are likely caused by the complex interactions between Li^+ ions and the functional group molecules. These interactions can influence the strength of the bonds within the functional groups, which can affect the vibrational modes of the functional groups and cause changes in the peak intensity and wavenumber in the spectrum.

The presence of $LiClO_4$ salt in PUA polymer matrix leads to a shift of the -NH stretching band to a higher wavenumber. This could be because Li^+ cations coordinated with nitrogen atoms in the N-H group then weaken the hydrogen bond of the -NH stretching and form polymer-salt complexation. This coordination causes the N-H bond to stretch at a higher frequency and results in the shift of the -NH stretching band to a higher wavenumber (Whba et al., 2020).

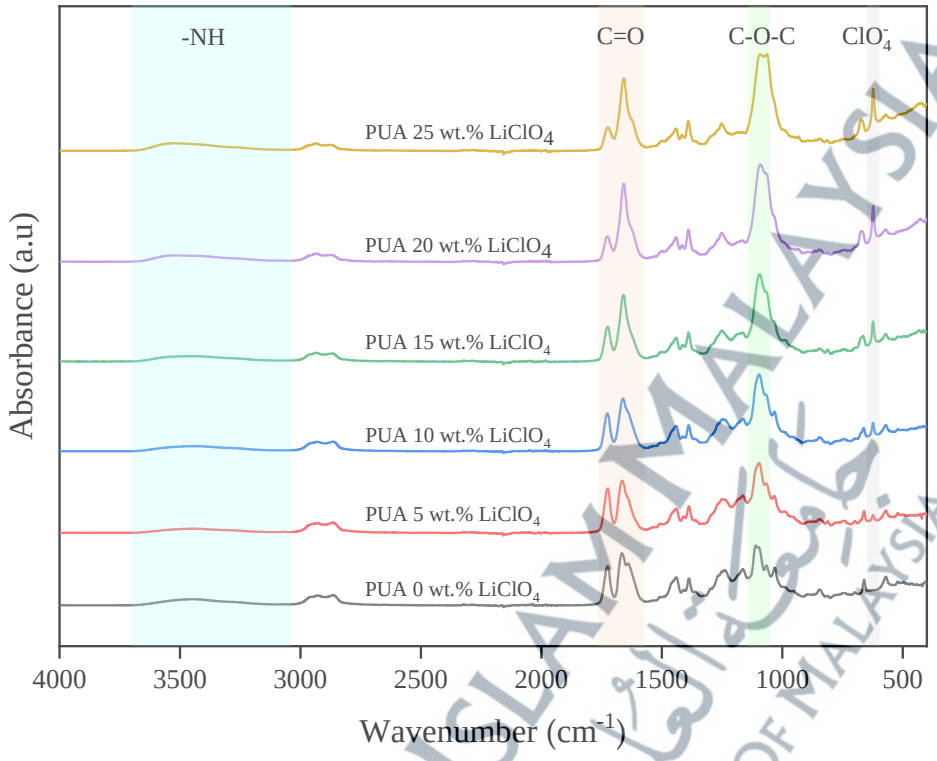

Figure 4.12: FTIR Spectra of PUA GPEs with Different $LiClO_4$ concentration (0-25 wt.%)

The carbonyl group (C=O) interacts with Li^+ cation in two wavenumbers which are 1723 cm^{-1} and 1666-1658 cm^{-1}. The peak at 1723 cm^{-1} is indicates to free -C=O groups and a free carbonyl group refers to a carbonyl functional group (-C=O) in a molecule that is not coordinated to a metal ion. The peak intensity increased as $LiClO_4$ concentration became higher. This is because of the increasing number of Li^+ ion that coordinate with free C=O decreasing the number of free carbonyl group thus decreased the peak intensity.

The peak 1666 to 1658 cm^{-1} could be assigned as the contribution of coordinated C=O groups in PUA. Coordinated carbonyl group is carbonyl group that having dipole interaction with Li^+ that forms a stable complex. The coordinated carbonyl group at peaks 1666-1658 cm^{-1} became more intense and shifted to a lower wavenumber which suggests

that more interaction of the carbonyl group with lithium salts and it weakened the C=O bond allowing the Li^+ cation to share electron density with oxygen atoms.

The oxygen ion in the carbonyl group in PUA plays a role as electron donor atoms and forms coordinate bonds with Li^+ cation in the polymer host structure (Naiwi et al., 2018). This coordination can happen through the donation of electrons from the electron-rich oxygen atom of the carbonyl group to the electron deficient Li^+ cation, forming a coordinate bond. The formation of this bond can cause a decrease in the electron density of the carbonyl group and thus lower its vibrational energy. As a result, the vibration frequency of the carbonyl group is shifted to a lower wavenumber in the FTIR spectrum, which is observed as a shift in the C=O stretching band to a lower wavenumber.

There was no peak shift occurred at 1097 cm^{-1} of C-O-C stretching band at did not show any shifting up to 10 w.t% $LiClO_4$. At 15% w.t, the peak starts slightly shifted to a lower wavenumber until it reached 1091 cm^{-1} for 25 w.t%. Besides, the band intensity also increased with the increasing salt content. This behavior can be explained by the strong interaction of the ether oxygen in the polymer matrix PUA with Li^+ cations. Li^+ cation is capable of coordinating with the PUA polymer, which can weaken the C-O-C groups. The coordination of Li^+ with the ether oxygen in PUA can cause a decrease in the electron density of the oxygen atom from the C-O-C bond, which frees some of the H-bonded ether groups. This can lead to a shift in the C-O-C stretching band to a lower wavenumber and an increase in its intensity.

These findings suggest that adding $LiClO_4$ salt to PUA causes multiple interactions that can change some of the polymer's microstructure. It also suggests that the $LiClO_4$ salt

can affect the hydrogen bonding interactions and the conformation of the PUA polymer, leading to changes in the FTIR spectrum.

Table 4.2: Free Ion and Ion Pairs of Different $LiClO_4$ Concentration

$LiClO_4$ content (w.t %)	Free Ion (%)	Ions Pair (%)
5	94.98	5.02
10	99.9	0.01
15	98.23	1.77
20	92.09	7.91
25	90.94	9.06

In order to gain insights into the interaction between the polymer matrix and lithium salt, FTIR deconvolution was employed. This method is used to analyze the absorption peaks of the infrared spectra and to separate the overlapping peaks, which can be attributed to different chemical groups or interactions. The information derived from the deconvolution of the absorbance peak can be attributed to the presence of both free ions and ion pairs (Licoccia et al., 2005)(Mustapa et al., 2016).

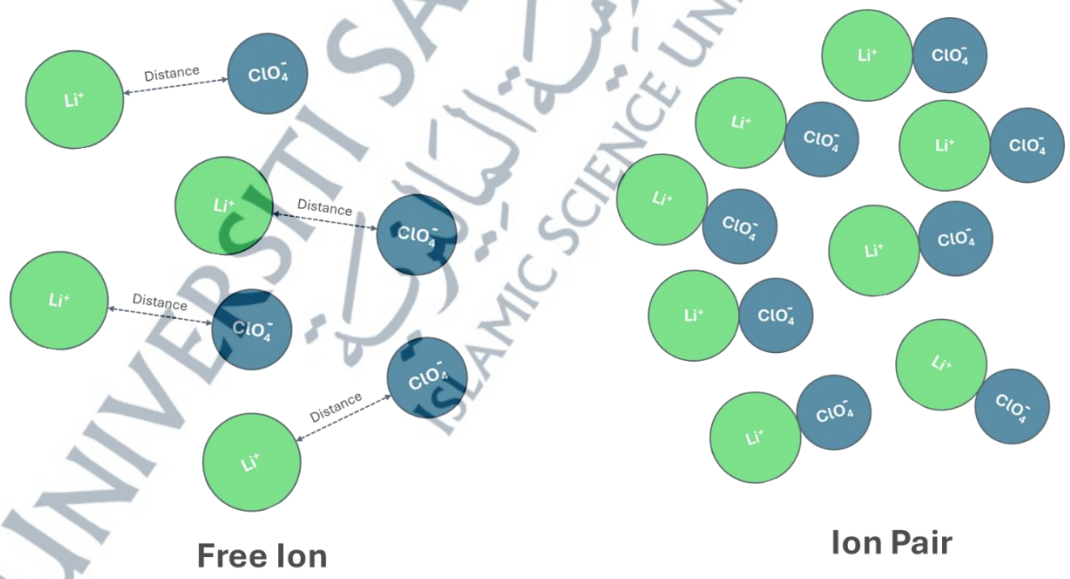

Figure 4.13: Free Ions and Ion Pairs of $LiClO_4$

Free ions refer to the ions that are mobile within the polymer matrix and are responsible for ionic conduction, meanwhile free ion refers to the combination of anions and cations that exist usually due high concentration of ion within the polymer matrix, causing insufficient distance between them caused by as shown in Figure 4.13.

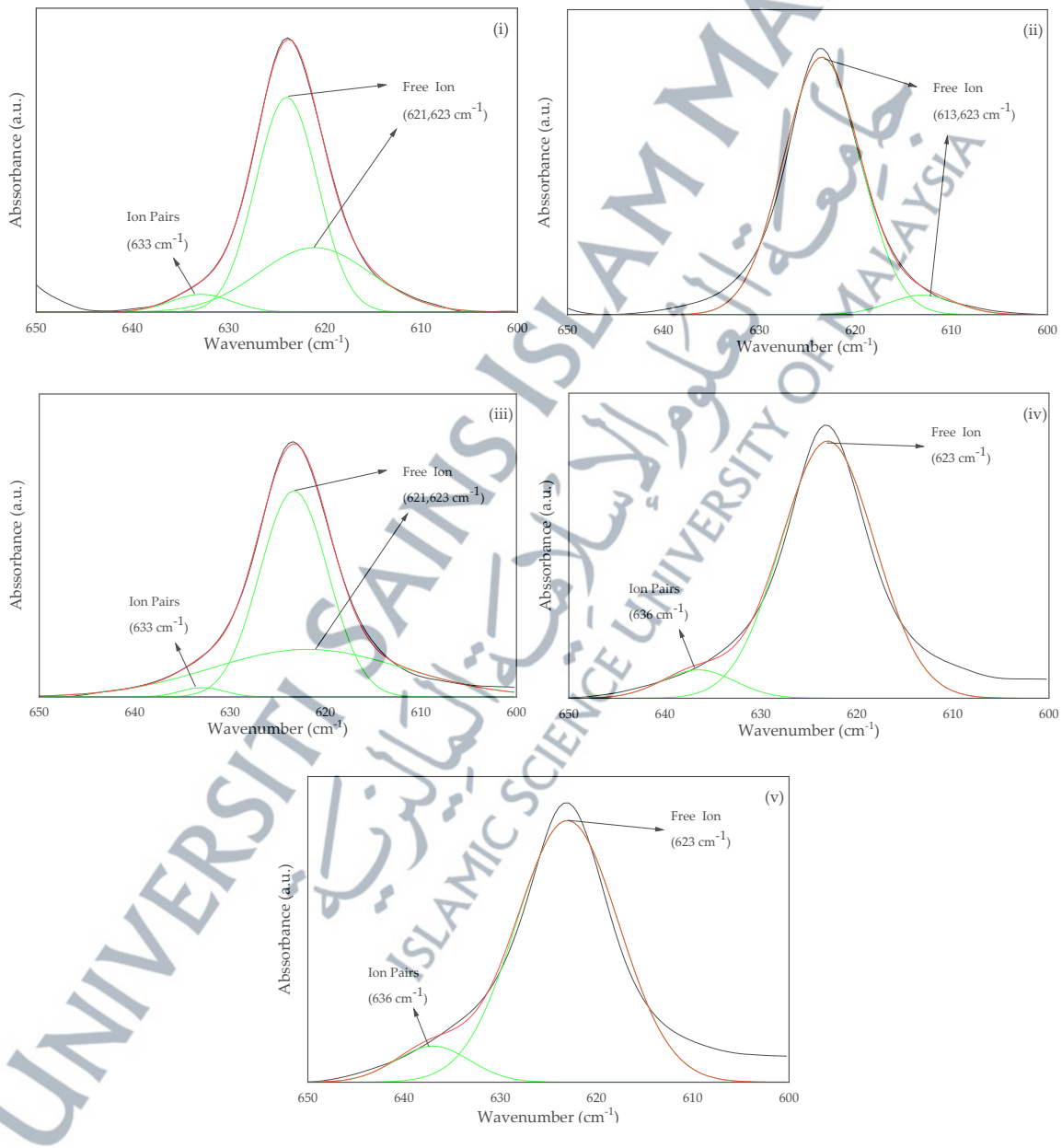

Figure 4.14: FTIR Deconvolution of $LiClO_4$ Peak (650 - 600 cm^{-1}). (i) 5 wt%, (ii) 10 wt%, (iii) 15 wt%, (iv) 20 wt% and (v) 25 wt%

Upon the addition of $LiClO_4$ to the polymer electrolyte, the FTIR analysis revealed new absorbance peaks at 616 and 633 cm^{-1}. These peaks were assigned to the presence of free ions and ion pairs in the electrolyte, as reported by Sim et al. (2010). Besides, other studies also proposed varying assignments for the peaks representing free ions and ion pairs of $LiClO_4$. In the study by Saikia et al. (2011), peaks at 624 cm^{-1} and 635 cm^{-1} were identified as free ions and ion pairs, respectively. Conversely, Tuan Naiwi et al. (2022) assigned 613 cm^{-1} and 614 cm^{-1} as free ions, while 633 cm^{-1} and 634 cm_{-1} were assigned as ion pairs of ClO_4-. These studies collectively suggest that the wavenumbers associated with free ions and ion pairs of $LiClO_4$ lie within the range of 650 to 600 cm^{-1}. The variations in peak assignments emphasize the need for further research and consensus among scientific investigations.

The FTIR deconvolution analysis results are visually represented in Figure 4.14, while the detailed numerical data and analysis are provided in Table 4.2 of the study. According to the obtained results, the peaks observed at 613 cm^{-1}, 621 cm^{-1}, and 623 cm^{-1} have been identified as indicative of free ions. On the other hand, the peaks detected at 633 cm^{-1} and 636 cm^{-1} have been attributed to ion pairs. These assignments are based on the analysis of the absorption peaks and the comparison with previous studies (Licoccia et al., 2005)(Sim et al., 2010).

The area under the graph of free ions and ion pairs was calculated using Equation 3.1 and 3.2 to study the percentage area of each species. Based on Table 4.2, the area percentage of free ion at 5 wt.% is 94.98% and increased to 99.9% at 10 wt.% of $LiClO_4$ concentration. The increasing number of free ions is due to the increasing concentration of $LiClO_4$ in the 3D printed GPEs sample. The results of this study suggest that the addition

of $LiClO_4$ salt promotes the generation of free ions, which are responsible for an increase in charge carriers and ionic conductivity.

However, When the concentration of $LiClO_4$ exceeds 10 wt.%, an interesting observation was made. The proportion of ion pairs increased from 0.01 wt.% to 9.06% at 25 wt.%. This indicates that as the concentration of $LiClO_4$ increases, the proportion of ion pairs in the material also increases, while the proportion of free ions decreases. This phenomenon can be explained by the fact that at higher concentrations of lithium salt, it becomes thermodynamically favorable for ion pairs to form rather than for free ions to dissociate. Hence, the preferential production of ion pairs over free ions occurs when the concentration of lithium salt is too high.

It was also observed that as the quantity of $LiClO_4$ was increased, more free ions were able to dissociate within the same volume of the polymer matrix. This makes sense since as the concentration of lithium salt increases, it becomes easier for free ions to dissociate from the ion pairs and become mobile. However, when the quantity of $LiClO_4$ reached a certain point, it became saturated. At this point, two free ions can merge and become neutral. This is the reason why the proportion of free ions decreases as the concentration of $LiClO_4$ increases. Overall, the concentration of $LiClO_4$ plays a crucial role in determining the proportion of free ions and ion pairs, which in turn affects the overall ionic conductivity of the material.

4.5 Transference Number Measurement (TNM)

The transference number measurement was conducted on 3D printed PUA GPE films with varying $LiClO_4$ concentrations (0 wt% to 25 wt%) to evaluate the extent of ion

contribution to the overall charge transport in the system. The behavior of all the samples, as shown in Figure 4.15, displayed a similar pattern. Initially, the normalized current decreased rapidly over time until it reached a steady state, characterized by a constant current level. This phenomenon is known as the steady state, where the ionic current across an ionic-blocking interface declines rapidly with time, indicating the predominance of ionic charge carriers in the electrolyte (Samsudin et al., 2012)

Table 4.3: Transference Number of The Samples

Samples	Transference Number		
	t_i	t_e	Total
5 wt% $LiClO_4$	0.93	0.07	1.00
10 wt% $LiClO_4$	0.98	0.02	1.00
15 wt% $LiClO_4$	0.97	0.03	1.00
20 wt% $LiClO_4$	0.97	0.03	1.00
25 wt% $LiClO_4$	0.96	0.04	1.00

According to the data presented in Table 4.3, the TNM values in the $LiClO_4$-PUA GPEs system exhibited distinct trends with varying concentrations of $LiClO_4$. At 5 wt.% $LiClO_4$, the TNM value was recorded as 0.93, indicating a relatively high proportion of ionic charge carriers within the electrolyte. The TNM value gradually increased to its highest value of 0.98 at 10 wt.% $LiClO_4$, suggesting a significant dominance of ion migration in the charge transfer process. However, beyond 10 wt.% $LiClO_4$, the TNM values started to decrease, reaching 0.96 at 25 wt.% $LiClO_4$ concentration.

These findings strongly suggest that the primary charge carriers within the $LiClO_4$-PUA GPEs are predominantly ions. The TNM values, which represent the fraction of total charge carried by the mobile species, closely approached unity, indicating a high degree of ionic conduction within the system. Notably, the highest TNM value achieved in this study,

0.98, aligns with previous research conducted by (Ahmad et al., 2012)(Kai Ling et al., 2019).

The significant value of TNM, reaching 0.98, indicates that the charge transfer mechanism in the $LiClO_4$-PUA GPEs system primarily relies on ionic migration. The contribution of electrons to the overall charge transfer process is considered negligible. These results further highlight the suitability of the GPEs for ionic conduction and support their potential application in various electrochemical devices, such as batteries, where efficient and predominantly ionic charge transport is desired.

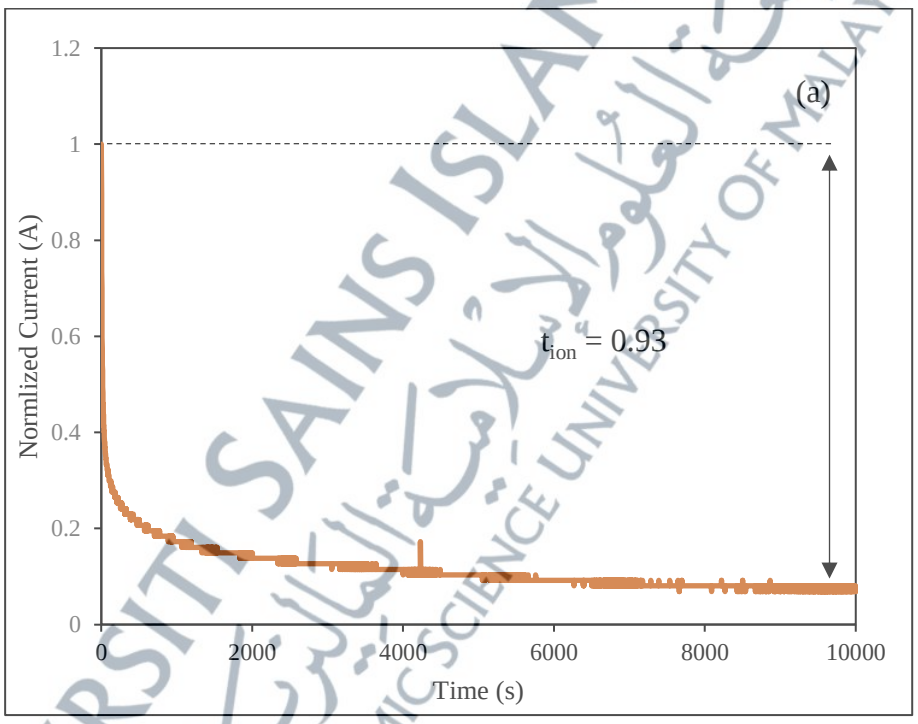

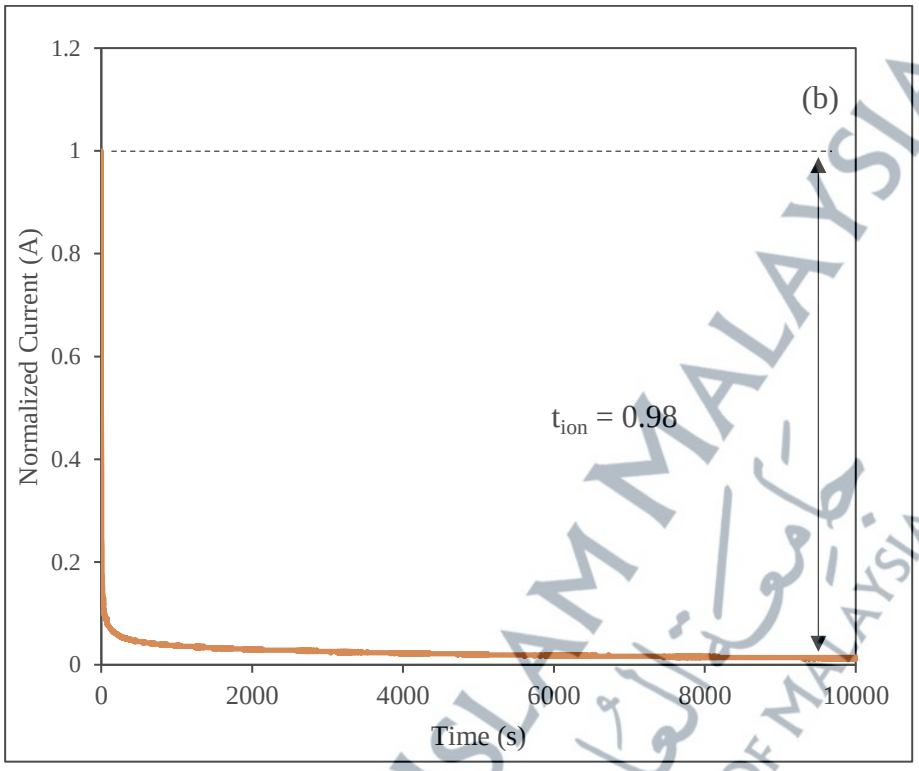

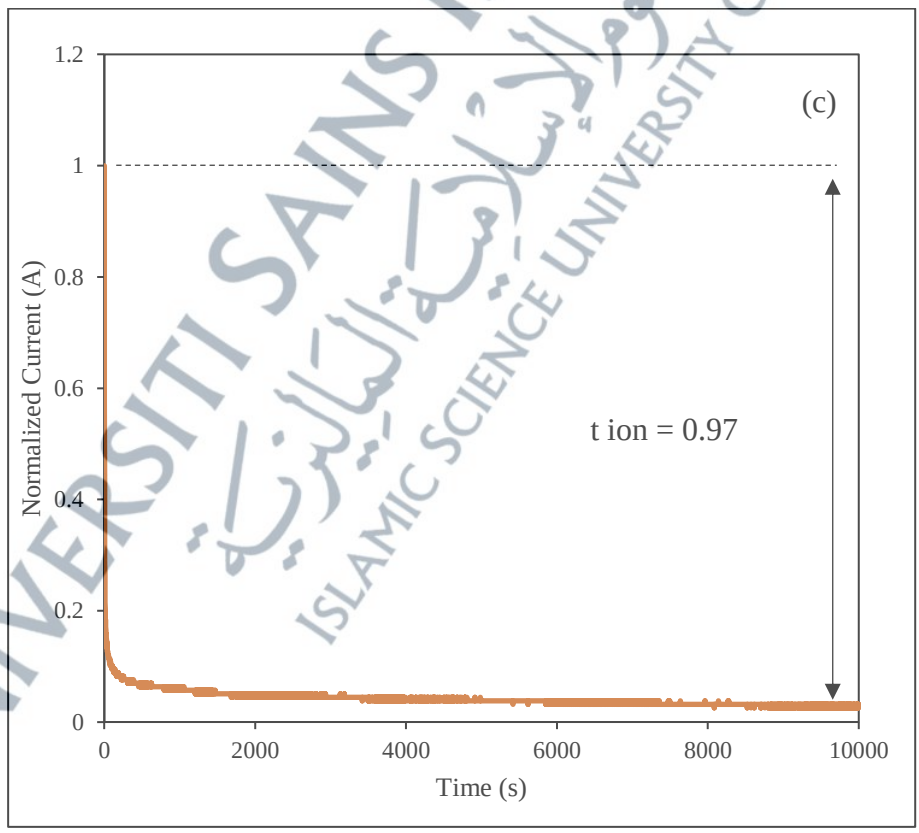

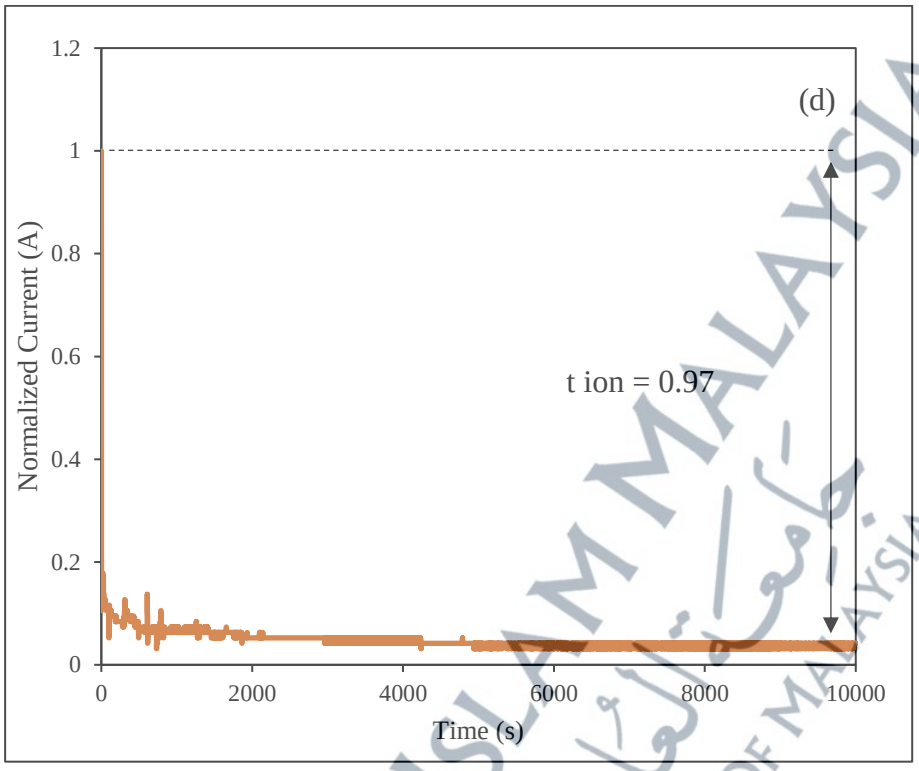

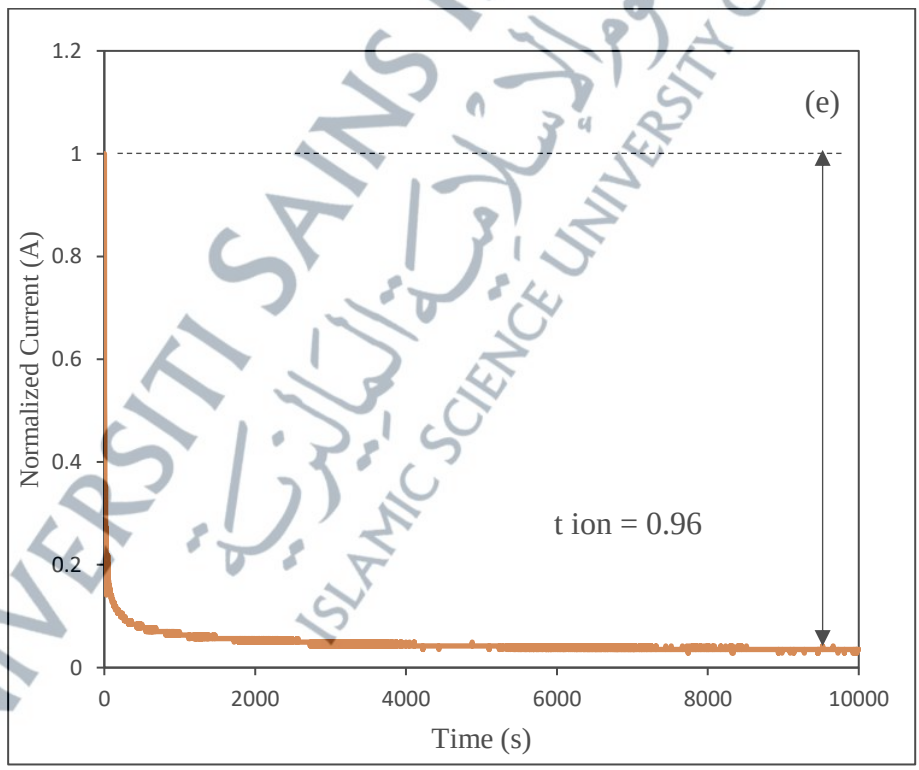

Figure 4.15: Normalized Current Versus Time of (a) 5 wt%, (b) 10 wt%, (c) 15 wt%, (d) 20 wt% and (e) 25 wt% $LiClO_4$ Samples

4.6 Electrical Impedance Spectroscopy (EIS)

EIS was deployed to investigate the electrical properties (ionic conductivity) of 3D printed PUA GPEs containing vary concentrations of $LiClO_4$ from 0% to 25 wt.%. The complex impedance plots of the GPEs were measured at room temperature and were represented as a combination of the real and imaginary parts of the Cole-Cole plot, Z' and Z'' as shown in Figure 4.16. The interception point of the real Z' axis was used to calculate the bulk resistance (Rb) of the samples. The bulk resistance is often used to calculate the conductivity of a material because it represents the resistance of the entire material, rather than just the surface or interface. The measured R_b values and the calculated ionic conductivity were then presented in Table 4.4.

From the Cole-Cole spectra plotted from 3D printed PUA GPEs in Figure 4.16, the bulk resistance of the samples decreases significantly with the addition of $LiClO_4$ from 59874 Ω at 0 wt%. to 68.38 ohm at 5 wt%. $LiClO_4$ concentration. After addition of another 5wt.% $LiClO_4$ to the sample, the bulk resistance reduced slightly to 14.94 Ω and further addition of salt did not reduce the bulk resistance. The bulk resistance and calculated ionic conductivity results are presented in Table 4.4. It was observed that the ionic conductivity of the PUA GPEs increased with increasing concentration of $LiClO_4$, until it reached a maximum conductivity of 1.24×10^{-3} Scm^{-1} at 10 wt.% $LiClO_4$. This conductivity value is four magnitudes higher than the conductivity of the GPEs containing 0 wt% $LiClO_4$, which was measured at 3.96×10^{-4} Scm^{-1}.

However, as the $LiClO_4$ concentration increased beyond 10 wt%, the ionic conductivity of the GPEs began to decrease to 8.83×10^{-4} Scm^{-1}, 6.06×10^{-4} Scm^{-1}, 4.88×10^{-4} Scm^{-1} for sample with 15 wt%, 20 wt.% and 25 wt.% $LiClO_4$ concentration

respectively. This trend can be attributed to the interaction between the quantity of charge carriers and the number of free ions (Santhosh et al., 2006). At higher salt concentrations, more lithium cations and perchlorate anions are present in the GPE matrix, which can lead to ion pairing. Ion pairing occurs when lithium cations and perchlorate anions associate with each other and form neutral species, reducing the number of free ions in the system.

It has been proven by the FTIR deconvolution results as the trend in the ionic conductivity results is consistent with the trend observed for the number of free ions and ion pairs in the FTIR deconvolution results. These findings suggest that the number of free ions is highly correlated with the ionic conductivity values as the higher the free ions, the higher the ionic conductivity values.

Besides, this trend also could be explained by number amorphous proportion within the GPEs from the FWHM in XRD analysis results. The sample that has the highest amorphous proportion was determined at 10 wt.% having the highest ionic conductivity value and the other sample results also show same pattern. This proves the direct relationship between amorphous proportions and ionic conductivity as the higher the amorphous region, the higher the ionic conductivity.

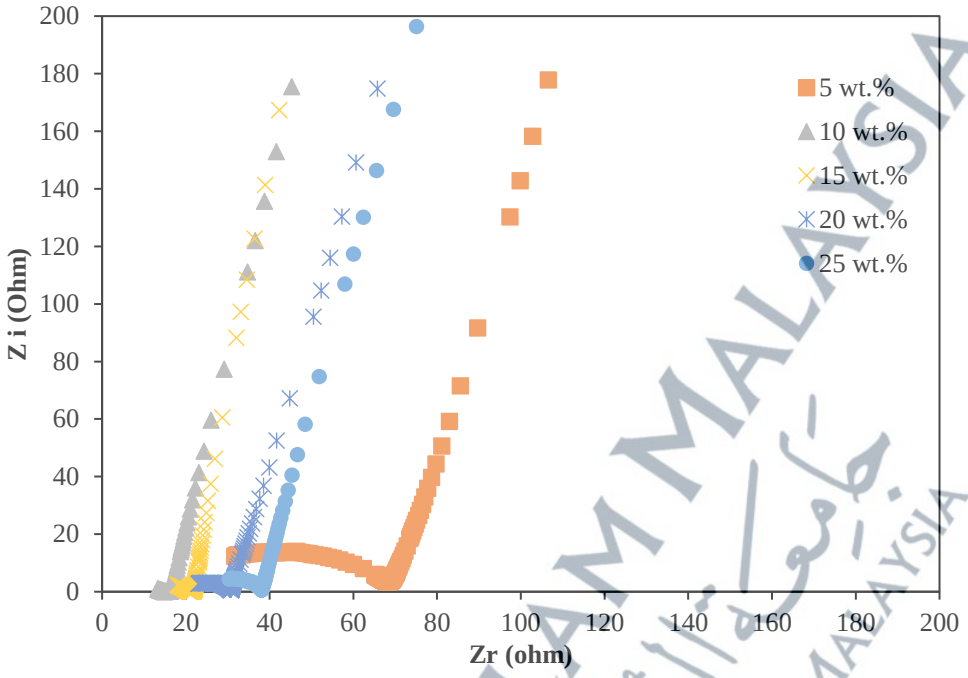

Figure 4.16: Cole-Cole Plot of SLA Printed PUA GPEs System

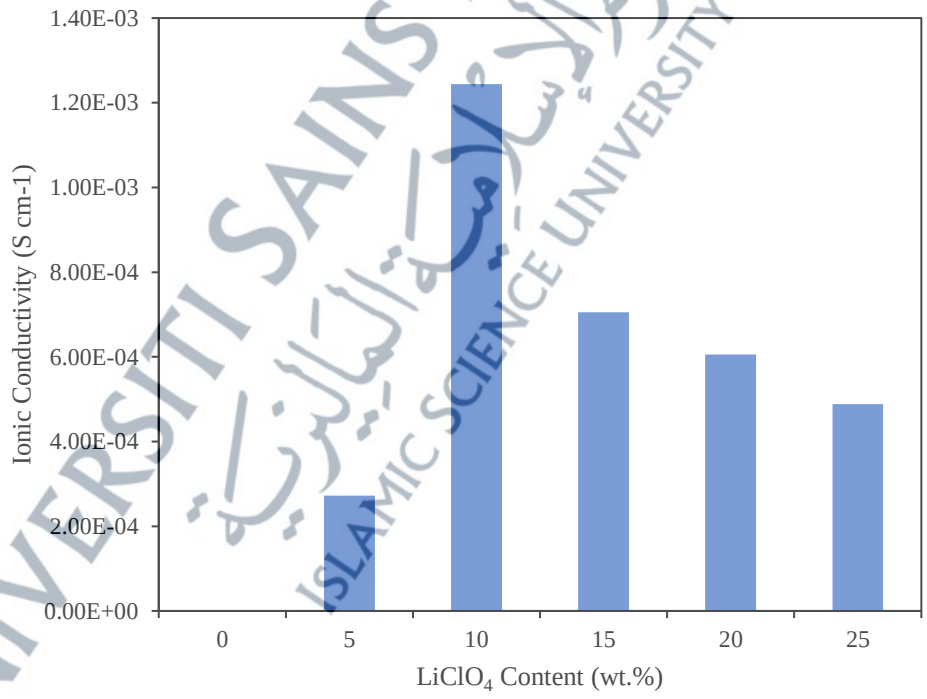

Figure 4.17: Ionic Conductivity of 3D Printed PUA GPE With Different Salt Concentration (0-25wt.%)

Table 4.4: Bulk Resistance and Ionic Conductivity of SLA Printed PUA GPEs

$LiClO_4$ (wt %)	Rb (Ω)	σ (Scm^{-1})
0	59874	3.11×10^{-11}
5	68.38	2.72×10^{-4}
10	14.95	1.24×10^{-3}
15	21.06	8.83×10^{-4}
20	30.71	6.06×10^{-4}
25	38.09	4.88×10^{-4}

The ionic conductivity of the samples also can be determined by using number density (n) and mobility (μ) of charge carriers as shown in equation below where e is electron charges (constant).

(4.1) $$\sigma = n\mu e$$

Based on the results from Figure 4.18(a), it suggests that increasing the concentration of $LiClO_4$ can enhance the number of charge carriers within the GPEs, as expected. However, Figure 4.18(b,c) indicates that this enhancement has a limited effect on the ionic conductivity, only up to 10 wt.% $LiClO_4$ concentration due to the decrease in mobility and diffusion coefficient of the charge carrier. This decrease in mobility and diffusion coefficient is explained by the higher rate of ion collision caused by the greater number of free ions within the GPEs (Shamsuddin et al., 2017). In other words, when the density of charge carriers is increased, the ions become more crowded and collide with each other more frequently. This collision slows down the movement of the charge carrier and reduces its diffusion coefficient, which ultimately results in limited enhancement of the ionic conductivity.

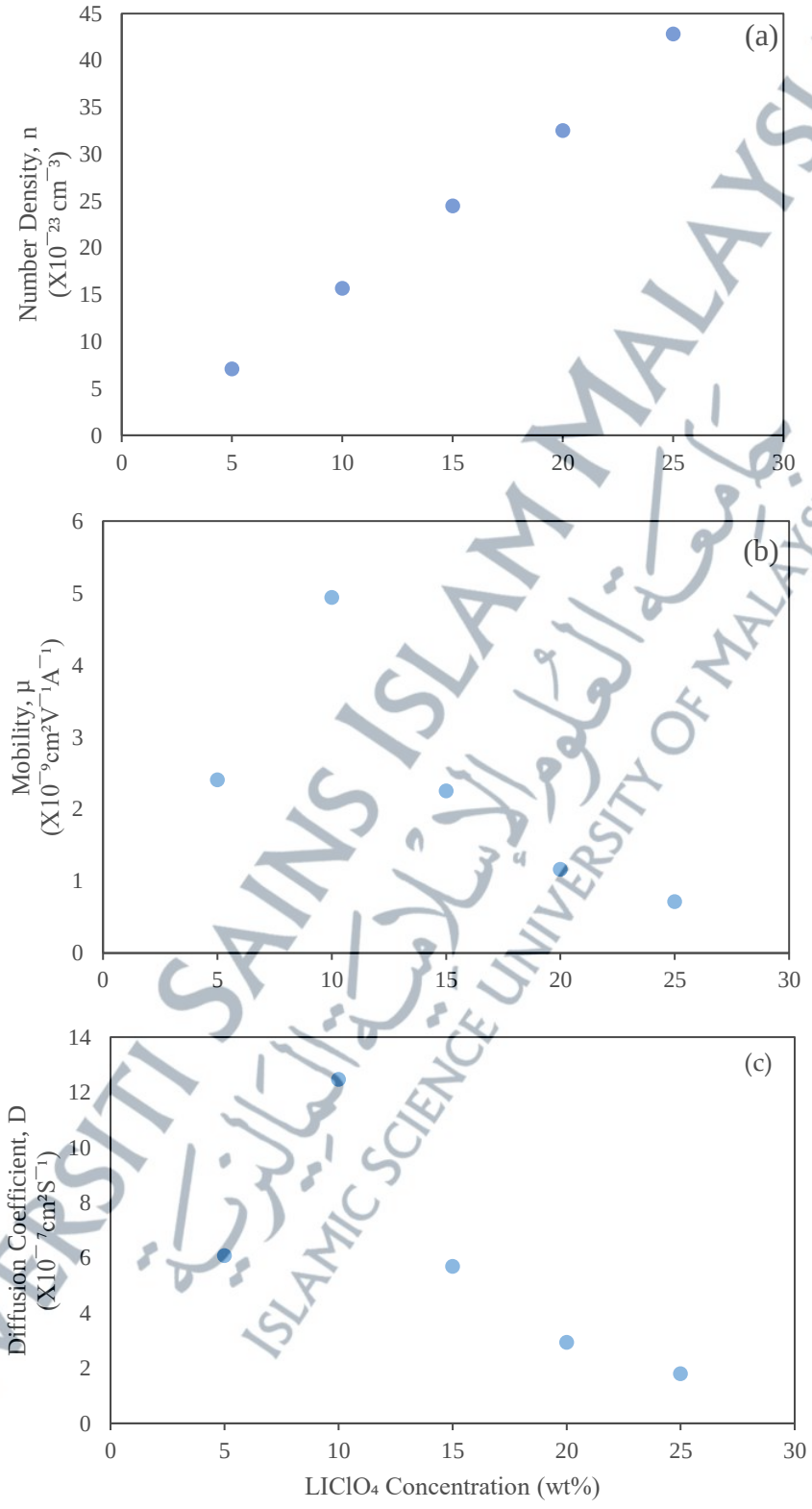

Figure 4.18: Number Density (n), Mobility (μ), and Diffusion Coefficient (D) of Different $LiClO_4$ Concentration

4.7 Dielectric Studies

Graphs in Figure 4.19 and Figure 4.20 illustrate the changes of dielectric constant (ε_r) and dielectric loss (ε_i) with frequency at room temperature for various concentrations of $LiClO_4$ in 3D printed PUA GPEs. The results showed that the values of ε_r and ε_i were higher at low frequencies and decreased as the frequency increased. The observed higher values of ε_r and ε_i at lower frequency can be attributed to a combination of ion polarization (Khiar et al., 2006) and space charge effect (Pradhan et al., 2008).

Ion polarization is a phenomenon that occurs in materials containing mobile charged particles, such as ions, in the presence of an electric field. When an electric field is applied to such a material, the charged particles tend to move and align themselves with the field direction, causing the material to become polarized. This polarization leads to an increase in the material's ε_r and ε_i.

At lower frequencies, the electric field oscillates more slowly, allowing the charged particles in the material more time to move and align themselves with the field direction. This results in a greater degree of ion polarization and a higher value of $\varepsilon_r$and ε_i.As the frequency increases, the electric field oscillates more rapidly, giving the charged particles less time to move and align themselves, resulting in a decrease in ion polarization and a corresponding decrease in $\varepsilon_r$and ε_i. Therefore, the higher values of $\varepsilon_r$and ε_i observed at lower frequencies are due to the greater degree of ion polarization in the material.

Meanwhile, the space charge effect is a phenomenon that occurs in materials with mobile charged particles, such as ions, when an electric field is applied. As the electric field is applied, charged particles within the material begin to move towards the electrodes,

creating a region of charged particles near each electrode. This region of charged particles is known as a space charge region.

The presence of space charge can distort the electric field within the GPEs that lead to a non-uniform distribution of the electric field strength. This distortion can affect the apparent dielectric constant measured in the material. The space charge region can effectively change the local dielectric constant, leading to an overall change in the measured dielectric constant of the GPEs.

Besides, the movement of charged particles in the space charge region can lead to energy dissipation, resulting in dielectric loss. This loss mechanism is particularly significant in materials with high ion mobility such as GPEs. The presence of space charge can enhance the dielectric loss of the GPE due to the increased movement of ions in the presence of an electric field.

According to the Figure 4.19 and Figure 4.20, the values of ε_r and ε_i were observed to be highest for the 10 wt% $LiClO_4$ concentration compared to the other concentrations. However, the values of ε_r and ε_i decreased beyond 10 wt% $LiClO_4$ concentration. This is because the 10 wt% $LiClO_4$ concentration has the highest value of free ions, charge carrier mobility, and diffusion coefficient, which contributes to ion polarization and space charge effect, resulting in higher values of ε_r and ε_i. The values of ε_r and ε_i decrease beyond 10 wt% $LiClO_4$ concentration due to a decrease in the number of free ions, charge carrier mobility, and diffusion coefficient.

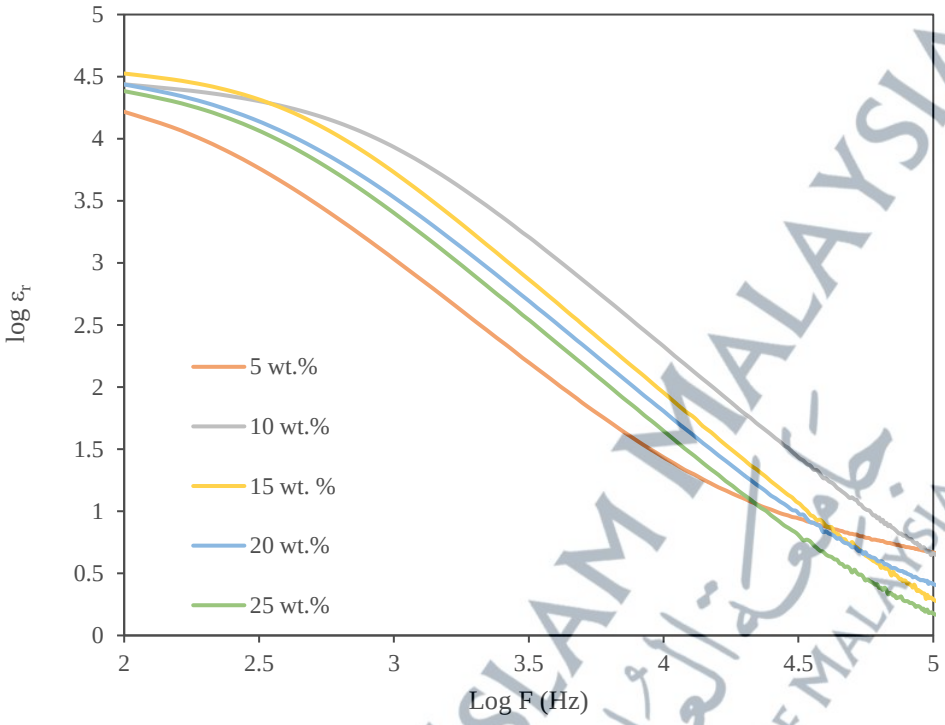

Figure 4.19: Log Dielectric Constant Versus Log Frequency

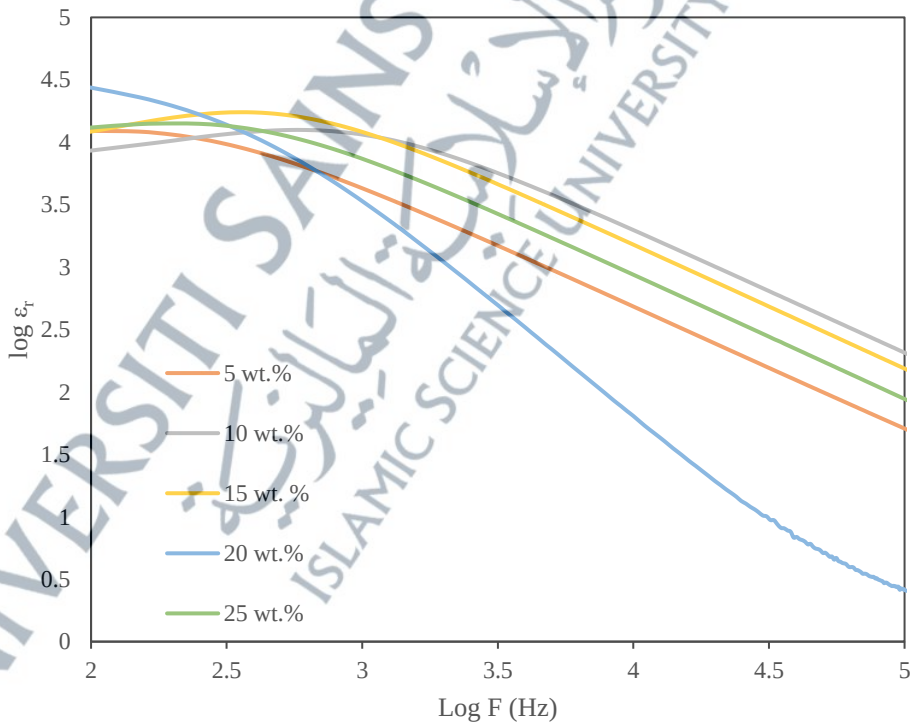

Figure 4.20: Log Dielectric Loss Versus Log Frequency

Figure 4.21 and Figure 4.22 provide summaries of the changes in the real electrical modulus (M_r) and imaginary electrical modulus (M_i) at various concentrations of $LiClO_4$ as a function of logarithmically scaled frequency. Notably, both M_r and M_i exhibit a notable increase that becomes significant within the frequency range of 4.5 Hz to 5 Hz. This indicates a distinct change in the electrical behaviour of the system within this frequency range that effected by different $LiClO_4$ concentrations.

The rapid rise in the values of M_r and M_i beyond 5Hz and 4.5Hz respectively can be attributed to the emergence of ion polarization and space charge effects, which become more prominent at higher frequencies. At lower frequencies, these effects have minimal influence on the dielectric properties of the material. However, as the frequency increases, the ions within the material align themselves with the electric field, resulting in increased polarization.

Additionally, the accumulation of charged particles at interfaces between different regions of the material gives rise to space charge effects. These phenomena contribute significantly to the values of M_r and M_i at higher frequencies, leading to a sharp escalation in their magnitudes beyond approximately 5Hz and 4.5Hz, respectively. According to Khiar et al., (2006), the findings suggest that the PUA GPEs samples produced through 3D printing exhibit the ability to function as ionic conductors as there were presence of charged particles that are crucial in enhancing the overall ionic conductivity of the material.

At low frequencies, the values of both M_r and M_i were observed to be close to zero, accompanied by a prolonged tail in the response. This behaviour can be attributed to the material having sufficient time to adequately respond to the applied electric field, resulting in little to no phase shift between the applied electric field and the material's response.

Additionally, the presence of a long tail suggests the presence of a significant capacitance associated with the electrodes, which is indicative of a slight polarization effect in the material. (Tuan Naiwi et al., 2022).

As the frequency of the applied electric field increases, the material exhibits a delayed response compared to the applied electric field, resulting in a phase shift between the two. This phenomenon causes an increase in the values of both the M_r and M_i. The lagging response and phase shift indicate that the material's ability to follow the rapidly changing electric field decreases, leading to a greater disparity between the applied field and the material's response, as evidenced by the higher values of M_r and M_i.

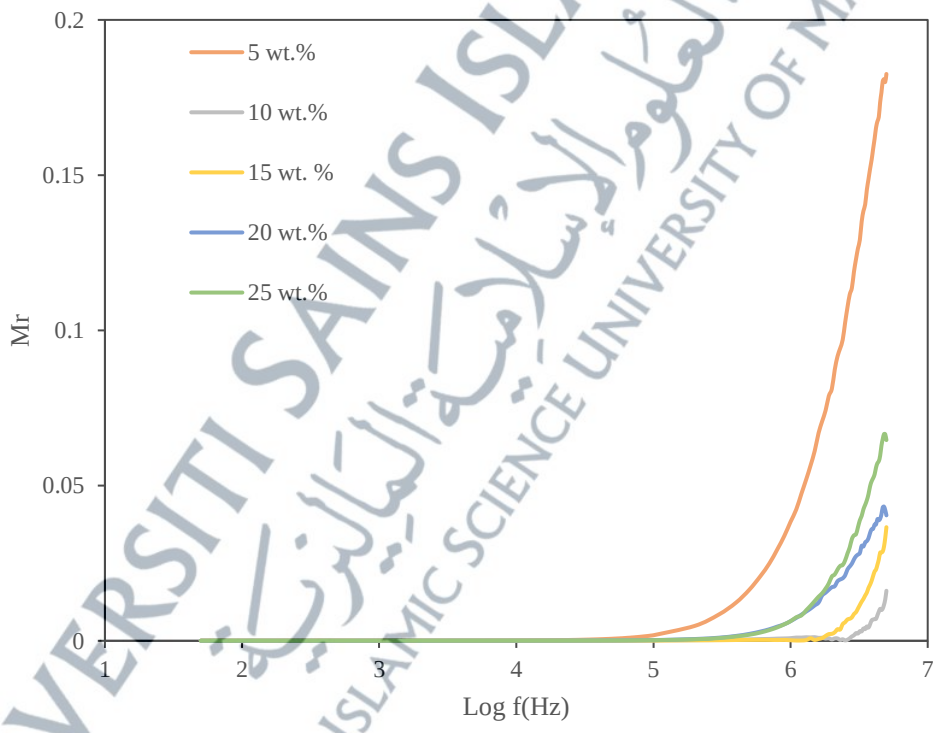

Figure 4.21: Real Part Electrical Modulus Versus Log Frequency

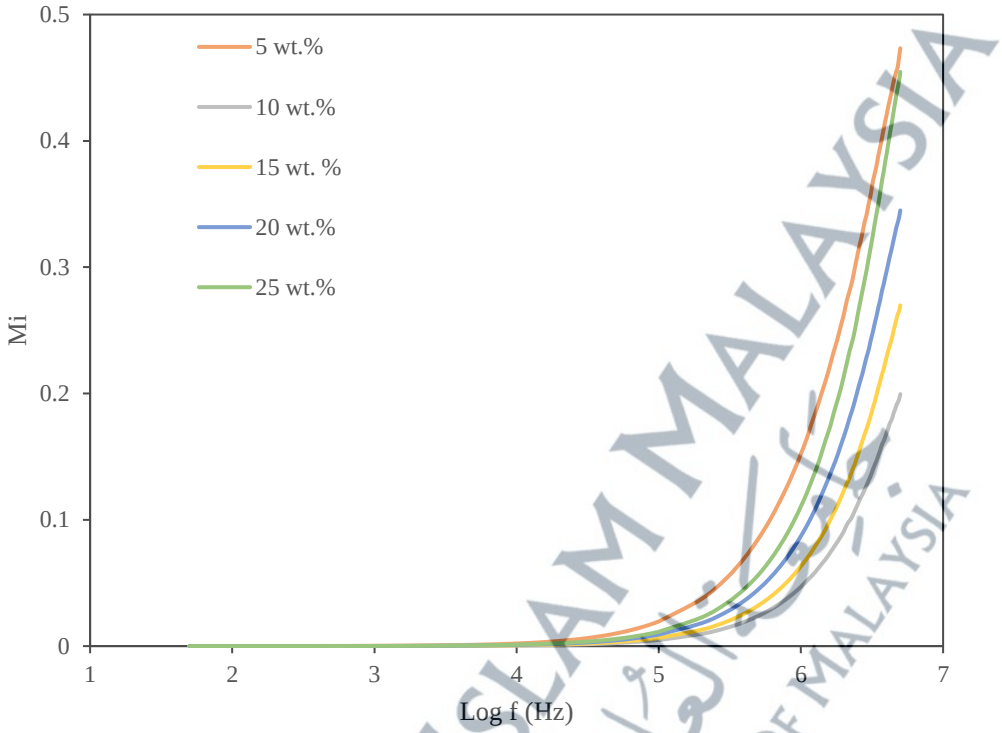

Figure 4.22: Imaginary Part Electrical Modulus Versus Log Frequency

Figure 4.23 displayed a plot illustrating the relationship between the tangent of conductivity (tan σ) and the logarithm of frequency. Each concentration of Lithium salt exhibited distinct peaks on the graph where the maximum peak can be determined. These peaks were utilized to calculate the relaxation time (τ) associated with each concentration. The presence of relaxation time indicates the existence of a relaxation parameter within the GPEs, suggesting the occurrence of relaxation processes within the material (Pradhan et al., 2008).

The graph exhibited notable peaks at higher frequencies, with the 10 wt% $LiClO_4$ concentration displaying the highest peak. It was observed that as the frequency increased, the corresponding relaxation time decreased. The relaxation time signifies the duration

required for ions to diffuse between electrodes. In essence, it is a measure of the time necessary for ions to travel from one electrode to another.

The relaxation time, as summarized in Table 4.5 for the 3D printed GPEs revealed intriguing findings. Remarkably, the lowest relaxation time of 6.37 $x10^{-08}$s was recorded for the 10 wt% $LiClO_4$ concentration. This aligns with the GPE achieving the highest conductivity among the tested samples. Consequently, it can be inferred that a shorter relaxation time corresponds to enhanced ionic mobility and conductivity within the GPEs.

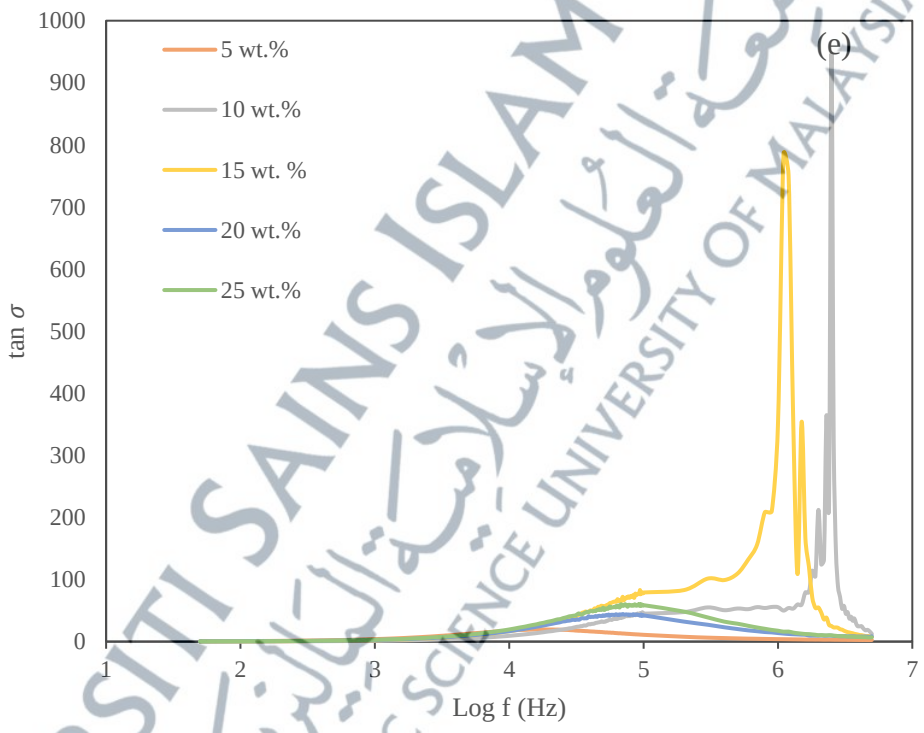

Figure 4.23: Tan σ Versus Log Frequency

Table 4.5: Maximum Peak tan σ and relaxation time (τ) of the GPEs derived from Figure 4.23

$LiClO_4$ (wt %)	Maximum Peak (Hz)	τ, (s)
5	4.20	$9.9x10^{-06}$
10	6.40	$6.37\ x10^{-08}$
15	6.04	$1.45\ x10^{-07}$
20	4.85	$2.27\ x10^{-06}$
25	4.97	$1.71\ x10^{-06}$

4.8 Thermogravimetric Analysis (TGA)

TGA was used to determine the thermal stability of the 3D printed GPEs, the temperature at which the electrolyte begins to decompose, and the amount of weight loss due to thermal degradation. According to Figure 4.24 and Table 4.6, the decomposition of the 3D printed GPEs for all the samples happened within two temperature ranges. The first decomposition (d1) occurred in temperature of 50°C up to 294°C and the second decomposition (d2) which was also the major decomposition occurred in temperature started from 294°C up to 336°C.

The first decomposition mainly occurred because of DMF evaporation from the 3D printed GPEs. Meanwhile, the second decomposition represented the degradation of PUA polymer chain. The value of d2 shifted to lower temperature as the concentration of $LiClO_4$ in the GPEs sample increased as shown in This happened because of the weakening carbonyl group due to decreasing number of electron density of oxygen in the C=O bonds that associate with Li^+ ions that form complexion (M. L. Digar et al., 2002) .

The decreasing D2 values over the increasing concentration could be due to several reasons. Firstly, higher $LiClO_4$ concentrations increase the number of lithium ions available promote more ionic interactions with the polymer matrix which weaken the polymer chains

and reducing overall stability. Secondly, $LiClO_4$ can act as a plasticizer that lowers the glass transition temperature (T_g) of the polymer and increases the molecular mobility which makes the polymer more prone to degradation at lower temperatures. Lastly, complex formation between $LiClO_4$ and the polymer chains can disrupt the polymer structure. The decreasing D2 value indicates lower thermal stability of 3D printed PUA GPEs as it cannot withstand higher temperature.

Besides, the decreasing mass loss of the sample with the increasing $LiClO_4$ is due high decomposition temperature of $LiClO_4$. At higher LiClO4 concentrations, more decomposition products of $LiClO_4$ might interact with the polymer matrix and forming more stable residues. These residues could remain behind during the analysis, leading to a lower overall mass loss compared to samples with lower $LiClO_4$ content. From the TGA analysis, it can be concluded that the addition of $LiClO_4$ into 3D printed GPEs decreased its thermal stability as less temperature is needed to decompose the polymer matrix of the GPEs.

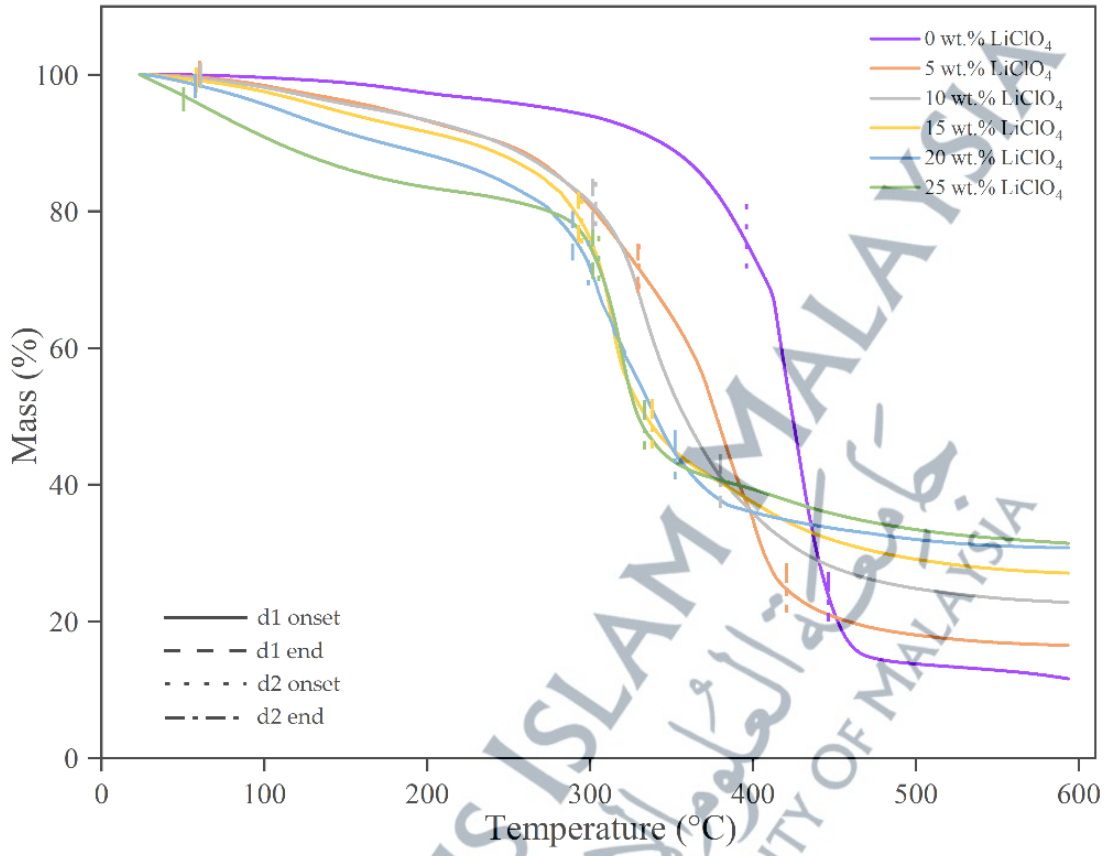

Figure 4.24: Thermograms of 3D Printed GPEs PUA With Different of $LiClO_4$ Concentration

Table 4.6:Thermogram Analysis of 3D Printed GPEs PUA

$LiClO_4$ Content	Decomposition stages	Degradation Temp (^OC)		Mass Loss (%)	Residue (%)
		Onset X	End X		
0 wt%	d1	-	-	82.373	12.56
	d2	396.98	447.68		
5 wt%	d1	59.8	330.17	77.873	16.82
	d2	330.17	419.44		
10 wt%	d1	60.3	301.3	73.701	23.04
	d2	302.39	382.32		
15 wt%	d1	58.2	294.00	65.064	27.28
	d2	294.76	336.95		
20 wt%	d1	57.50	289.05	69.21	30.79
	d2	299.45	352.05		
25 wt%	d1	51.49	302.12	68.59	31.41
	d2	304.5	332.98		

4.9 Differential Scanning Calorimetry (DSC)

Figure 4.25 and Table 4.7 shows the thermal analysis of a 3D printed polymer electrolyte in the form of DSC thermograms. The polymer electrolyte samples were prepared with varying concentrations of $LiClO_4$, ranging from 0 wt.% to 25 wt.%. The data obtained indicates that the polymer electrolyte sample without $LiClO_4$ (0 wt.%) exhibited a glass transition temperature (T_g) of 18.60 ^oC, which aligns closely with the T_g value reported for PUA in a previous study (Liao et al., 2012). Notably, all the samples including the one without $LiClO_4$ demonstrated a singular T_g value and an endothermic melting peak, while no exothermic crystalline peaks were observed. These findings strongly suggest that all the samples possessed an amorphous structure, consistent with the XRD data. The incorporation of lithium salt into the polymer electrolyte led to an increased T_g value across all samples.

The inconsistency of the DSC result pattern compared to the ionic conductivity, FTIR deconvolution and FWHM XRD could be because of the temperature differences during the testing. All the results were obtained in room temperature meanwhile the T_g were detected at temperature below -15 ^oC. This situation might affect the consistency of the results as the magnitude or type of interaction between the ion and polymer matrix of two different temperatures might be different.

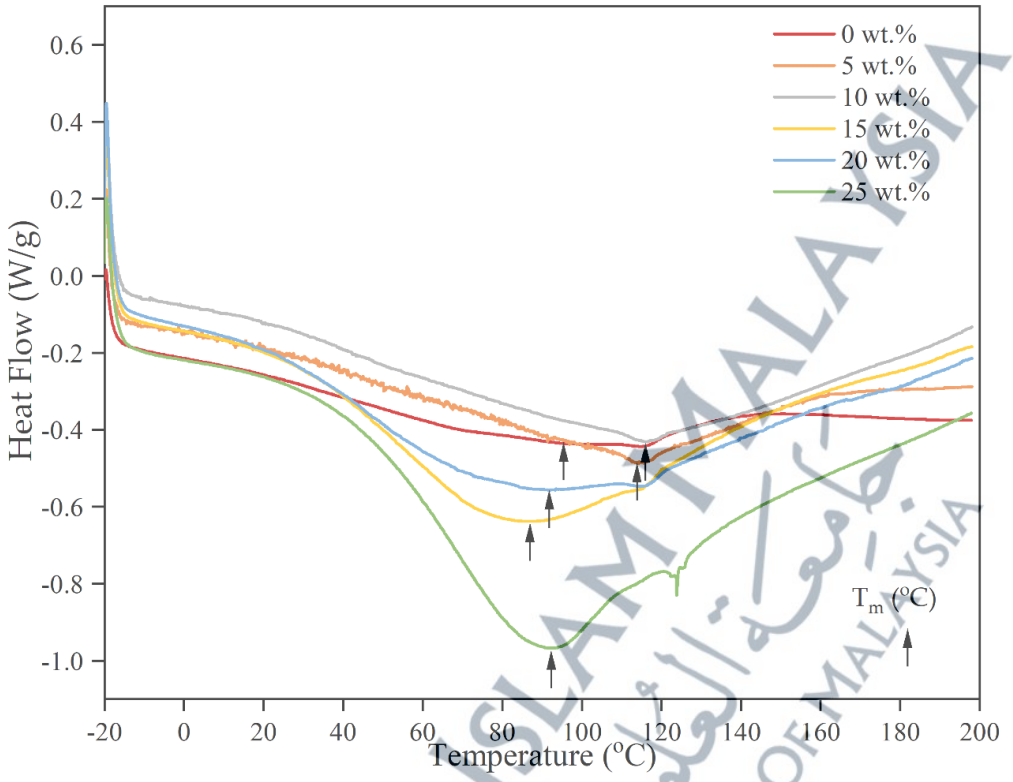

Figure 4.25: DSC thermograms of 3D Printed PUA GPE With Different $LiClO_4$ Concentration

The rise in T_g value resulting from the introduction of Li salt into the 3D printed polymer electrolyte can be elucidated through two underlying mechanisms. Firstly, the coordination between Li cations and the polyether oxygen atoms in the PUA chain restricts the mobility of polymer segments, consequently promoting a higher number of cross-linking interactions within the system. This increased cross-linking contributes to the elevated T_g value observed. Secondly, the ion-dipole interaction between Li ions and the polyester oxygen atoms of PUA induces a stiffening effect on the polymer chain. As a result, the polymer chain exhibits reduced flexibility, leading to an increase in the T_g value. These mechanisms align with a previous study that reported a similar correlation between

the addition of Li salt to a polymer electrolyte and an elevated T_g value (Lee et al., 2017)(M. Digar et al., 2001)(Mohanlal Digar & Wen, 2000).

Table 4.7: T_g and T_m Values of Different $LiClO_4$ Content 3D Printed PUA GPEs

$LiClO_4$ Content	T_g (°C)	T_m (°C)
0 wt%	-18.60	95.01
5 wt%	-18.55	114.00
10 wt%	-18.48	115.85
15wt%	-18.44	86.30
20 wt%	-18.46	91.55
25 wt%	-18.35	92.77

Moreover, the incorporation of lithium salt into the polymer electrolyte resulted in a notable impact on the melting temperature (T_m) of the samples. Specifically, the T_m value exhibited an increase up to a concentration of 10 wt%, followed by a subsequent decrease beyond this threshold. This behaviour can be attributed to the interaction of free ions with the hydrogen bonds present in the -NH chain of the polymer. As the concentration of lithium salt increases, the presence of free ions strengthens the intermolecular bonds, thereby elevating the T_m value. This phenomenon can be understood as the enhanced interaction between the ions and the -NH chain reinforces the intermolecular forces within the polymer structure.

However, beyond the 10 wt% concentration, the T_m value demonstrated a decline. This decrease can be attributed to the growing number of ion pairs within the system. At higher concentrations of lithium salt, caused the weakening of the dipole-dipole interaction between the PUA chains$^+$. Consequently, the intermolecular bonding may be weakened, leading to a reduction in the T_m value. In essence, the excessive formation of ion pairs may

hinder the favourable interactions between the polymer chains, resulting in a diminished T_m value beyond the 10 wt% concentration of lithium salt.

In summary, the polymer electrolyte exhibits three key interactions that significantly influence its properties. Firstly, there is an interaction between the ether oxygen groups and Li^+, resulting in the formation of transient cross-links. These cross-links restrict the segmental motion of the polymer chains, thereby affecting their mobility. Secondly, the urethane -NH and carbonyl groups also interact with Li cations, leading to intramolecular cross-linking. This interaction further limits the mobility of the polymer chains and affects their overall flexibility. Lastly, the mixed ether-urethane groups interact with Li^+, resulting in a two-phase system composed of hard and soft segments. These interactions contribute to the mechanical and thermal properties of the polymer electrolyte.

Collectively, these interactions within the polymer electrolyte have a significant influence on its behavior. They affect the mobility of the polymer chains, determine the extent of cross-linking, and contribute to the overall structure and composition of the electrolyte.

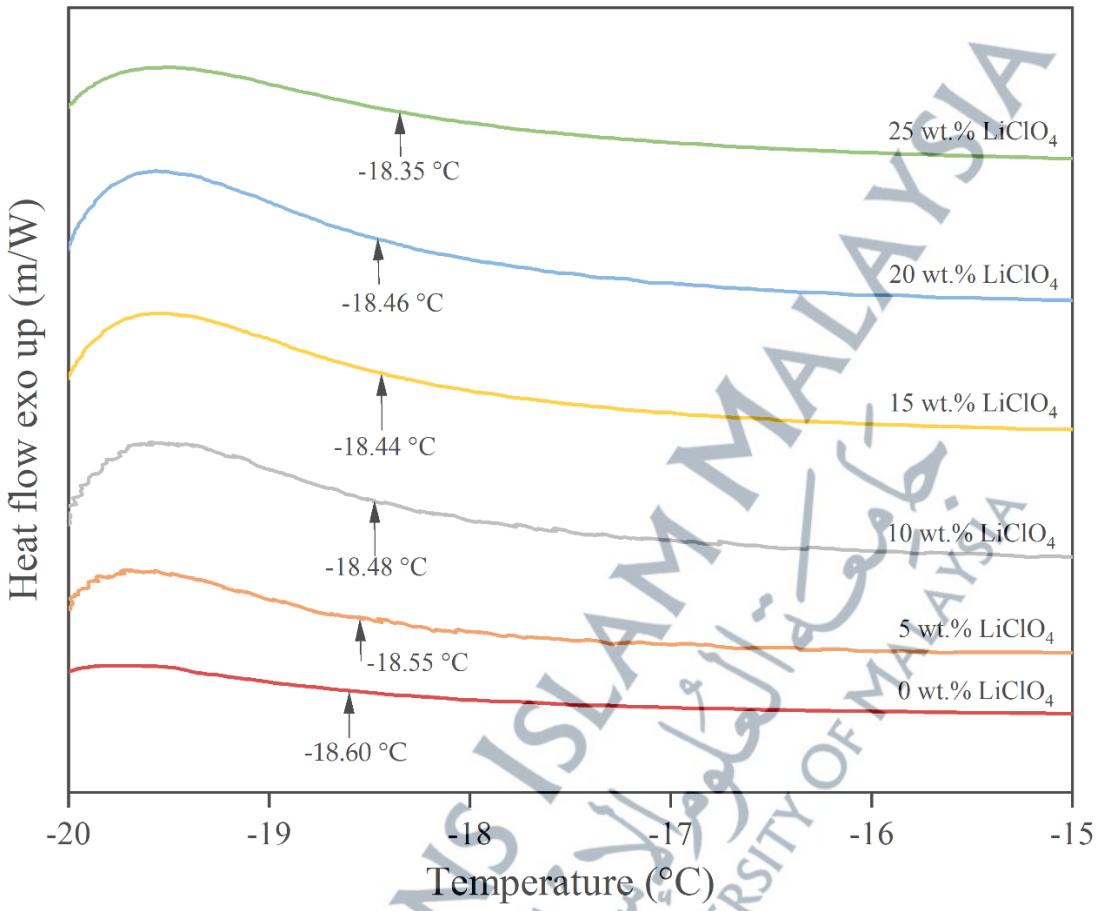

Figure 4.26: Glass Transition Temperature (T_g) of Different $LiClO_4$ Concentration 3D Printed PUA GPEs

4.10 Printability Validation

As the best formulation that produces the best performance in term of ionic conductivity has been determined at 10 wt.% $LiClO_4$ concentration, the formulation was printed into 3 different complex structures to validate its printability into 3D model designs instead of only 2D film. The printability validation was successfully as the 10 wt.% was successfully printed into honeycomb pattern, interdigitated structures and scaffold structures as depicted in Figure 4.27, Figure 4.28, and Figure 4.29. All the printed 3D

structures PUA GPEs have good mechanical properties with precise dimensions compared to the CAD designs dimensions.

This result means that researchers can push the boundaries of traditional electrolyte or battery design into 3D structures designs. The ability to fabricate GPEs into intricate and customized shapes broadens the possibilities for evaluating and analyzing battery performance. Researchers can now examine the effects of different geometries and structures on battery efficiency, opening up more space for innovation and breakthroughs. This new 3D printing technology for batteries marks the start of a fresh era in battery research. It opens doors for more progress in energy storage and clears the path for future use across different industries.

Figure 4.27: Honeycomb Pattern 3D Printed PUA GPEs

Figure 4.28: Interdigitated Structure 3D Printed PUA GPEs

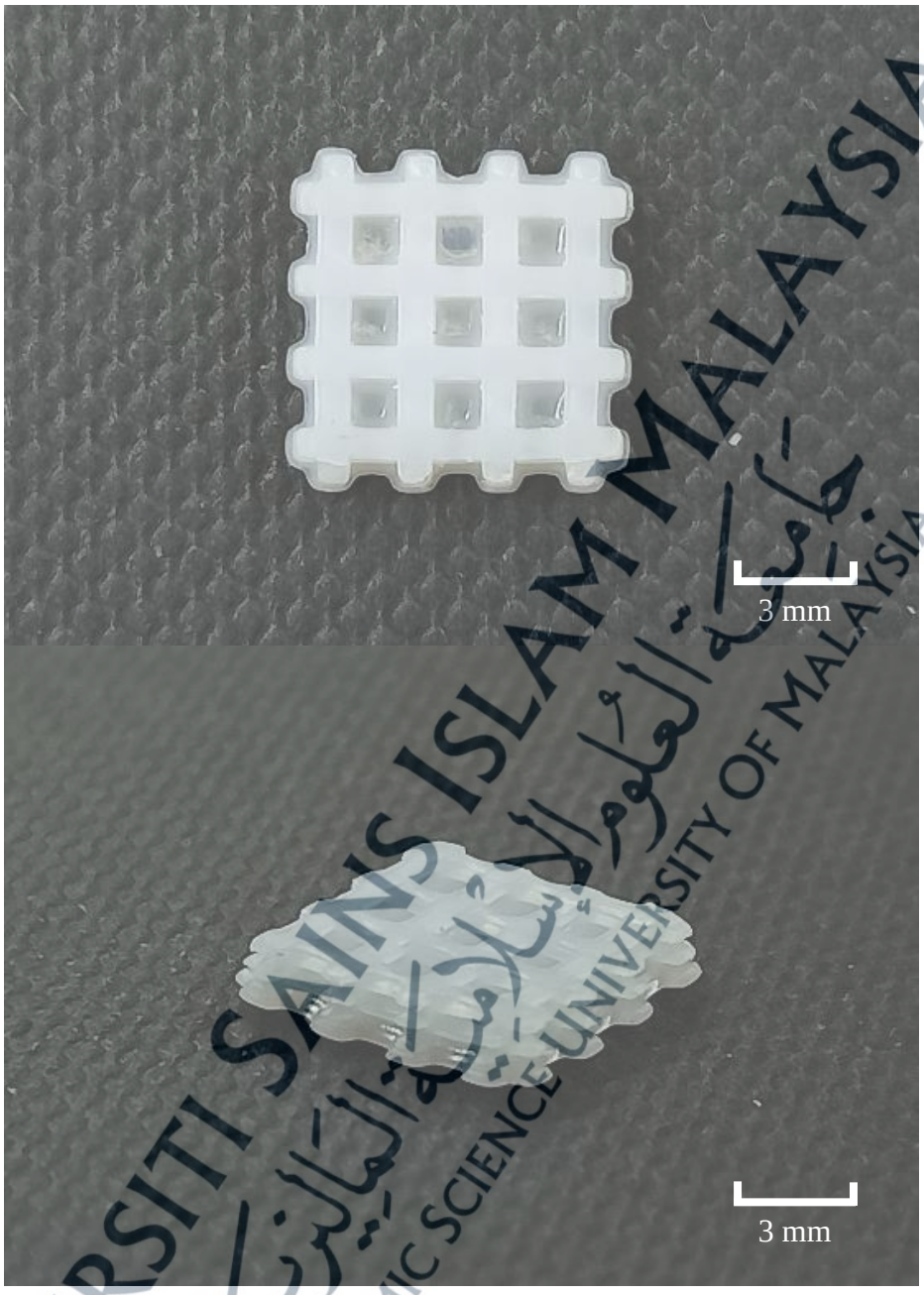

Figure 4.29: Scaffold Structure 3D Printed PUA GPEs